

ON THE EVIDENCE FOR DISCS AROUND BLUE STRAGGLER STARS

JOHN M. PORTER

Astrophysics Research Institute, Liverpool John Moores University, Twelve Quays House, Egerton Wharf, Birkenhead, CH41 1LD, UK

AND

R. H. D. TOWNSEND

Bartol Research Institute, University of Delaware, Newark, DE 19716, USA

Department of Physics & Astronomy, University College London, Gower Street, London, WC1E 6BT, UK

Received: 7th October, 2004, Accepted: 16th March, 2005

ABSTRACT

Recent observations of blue stragglers by De Marco et al. (2004) have revealed continuum deficits on the blue side of the Balmer discontinuity, leading these authors to infer the presence of discs around the stars. This intriguing possibility may throw light on aspects of the mechanisms responsible for at least some of these objects; current theories of blue straggler formation invoke stellar collisions or interacting binaries, both of which appear capable of forming a circumstellar disc.

However, by synthesizing photospheric spectra for models of rotating blue stragglers, we demonstrate that the Balmer jump enhancements can be wholly attributed to the influence of oblateness and gravity darkening on the formation of the continuum. Therefore, we are led to conclude that the observations of De Marco et al. can be ascribed a more prosaic explanation, that of rapid stellar rotation arising from the merger/interaction formation process.

Subject headings: blue stragglers – stars: rotation – stars: atmospheres – techniques: spectroscopic

1. INTRODUCTION

Blue stragglers (BSs) are cluster stars having anomalous evolutionary histories. They are blue stars of intermediate mass (a few M_{\odot} , Shara et al. 1997), with typical surface temperatures of $\sim 6,000$ – $10,000$ K (e.g., Deng et al. 1999). Application of single-star evolution theory indicates an age too young to be explained by the age of their parent cluster (see the review by Livio 1993, and references therein). This apparent paradox has been explained by two production paths for BSs: (i) collisions between two lower-mass stars (e.g. see the simulations by Sills et al. 2001), and (ii) mass transfer in moderately wide binary stars (e.g., Bellazzini et al. 2002). Both of these processes are likely to cause the remnant BS to spin up. Population studies of BSs have shown that both of these routes may be necessary to account for the observations (Davies et al. 2004).

Recently, De Marco et al. (2004, hereinafter DM04) have presented Hubble Space Telescope (*HST*) observations of BS spectra, and have argued that they detect the signature of a circumstellar disc around some of their targets. Disc formation is a common theme in BS generation and hence the DM04 observations could shed light on the different evolutionary processes responsible for these objects. The evidence advanced for the presence of discs rests largely on an apparent continuum deficit (by ~ 5 – 10%), falling on the short wavelength side of the Balmer discontinuity; DM04 interpret this deficit – and the corresponding *enhancement* in the magnitude of the Balmer jump – as arising from circumstellar absorption by the presumed disc.

On account of their putative formation mechanisms, BS are expected to exhibit moderate to high rotation rates. In this letter we investigate the effect of such rapid

rotation on the photospheric continuum, by developing a spectral synthesis model that correctly accounts for the oblateness and gravity darkening arising from the centrifugal force. We describe the model in §2, and use it in §3 to explore the evolution of the Balmer jump as the rotation rate is varied. In §4 we then apply the model to the blue straggler M3-17, demonstrating that it can successfully reproduce the observations by DM04. We discuss and summarize our findings in §5.

2. THE SPECTRAL SYNTHESIS MODEL

In a non-rotating, spherical star, the atmosphere across the entire surface may be characterized by a single value each for the effective temperature T_{eff} and gravity g . With the introduction of rotation, however, the outward pull of the centrifugal force distorts the star into an oblate spheroid. Across the surface of this spheroid, the effective gravity g_{eff} (composed of the vector sum of the Newtonian gravity and the centrifugal acceleration) is non-uniform, decreasing toward the equatorial regions where the centrifugal force is strongest. Likewise, in accordance with the gravity darkening law of von Zeipel (1924), the effective temperature decreases toward the

equator in accordance with the relation $T_{\text{eff}} \propto g_{\text{eff}}^{\frac{1}{4}}$.

To model such an oblate, gravity-darkened star, we set up a raster grid that divides the surface¹ into c. 14,000 pixels², each covering an area $0.015 R_p$ square, where R_p is the star’s polar radius. We calculate the local effective gravity associated with the surface point to which each pixel corresponds, and we likewise assign a local effective

¹ Defined by an isosurface of the effective potential within the Roche approximation (see, e.g., Cranmer 1996).

² The exact number of pixels composing the surface varies with the degree of centrifugal distortion of the star.

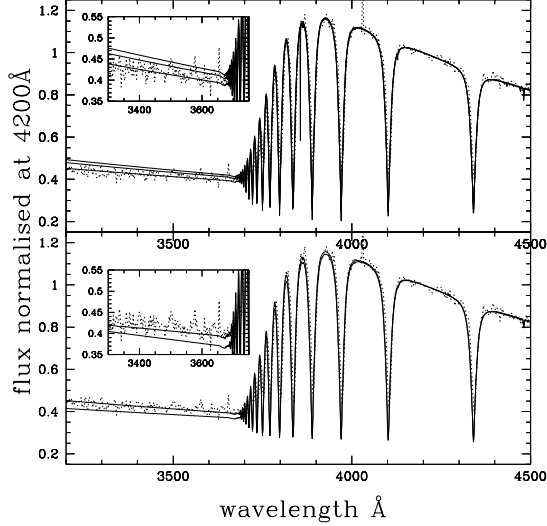


FIG. 1.— Synthetic spectra from rotating stars: the top panel shows a non-rotating model, and (decreasing downward for wavelengths less than 3700 Å) models for $v_{\text{eq}}/v_{\text{crit}} = 0.3$ and 0.5, while the lower panel have models for $v_{\text{eq}}/v_{\text{crit}} = 0.7$ and 0.9 (increasing upward). All models are equator-on (inclination $i = 90^\circ$). The insets are the models presented over a smaller wavelength range to highlight the flux shortward of the Balmer Jump. The dotted line on all panels shows the spectrum of M3-17.

temperature

$$T_{\text{eff}} = \left(\frac{4\pi R_p^2 g_{\text{eff}}}{\Sigma_1} \right)^{\frac{1}{4}} T_{\text{eff},0}, \quad (1)$$

following von Zeipel's law. The overall normalization of these temperature data is specified by the notional effective temperature $T_{\text{eff},0}$ that the star would have if it were non-rotating, under the (reasonably-accurate) ansatz that the stellar bolometric luminosity remains invariant as the rotation rate changes. The symbol Σ_1 denotes the surface-area weighted gravity of the distorted star, which depends amongst other things on the rotation rate (see equations 4.22–4.24 of Cranmer 1996).

Knowing the effective temperature and gravity of each pixel, and furthermore the local projection cosine μ of the surface normal onto the line of sight, we interpolate the observer-directed emergent flux in a $T_{\text{eff}}-\log g-\mu$ grid of precomputed angle-dependent intensity spectra. By co-adding the flux data from all pixels, weighted by their projected area $(0.015R_p)^2$ and Doppler shifted by the line-of-sight velocity due to rotation, we thereby build up a disc-integrated spectrum for the entire distorted, gravity-darkened star. For the calculations presented in the following section, we adopt an intensity spectrum grid calculated using the SYNSPEC spectral synthesis code of I. Hubeny and T. Lanz. The spectra incorporate lines due to H, He, C, N, O, Si, Mg, and Ne, and are based on the am20ak2-odfnw grid of line-blanketed LTE model atmospheres published by Kurucz (1993) (these have H/He = 0.34 by mass and are alpha enhanced by 0.4dex and metal depleted by 2.0dex).

3. INFLUENCE OF ROTATION ON THE BALMER JUMP AND COLORS

In Fig. 1 we present synthetic spectra covering the wavelength range 3,200–4,500 Å, calculated for equatorial rotation rates $v_{\text{eq}}/v_{\text{crit}} = 0.0, 0.3, 0.5, 0.7$ and

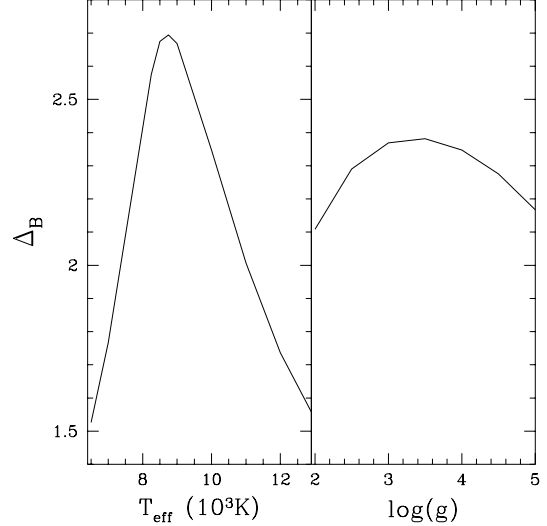


FIG. 2.— The Balmer jump magnitude Δ_B plotted as a function of effective temperature at fixed $\log g = 4.0$ (left), and as a function of gravity at fixed $T_{\text{eff}} = 10,000$ K (right).

0.9 using the model we describe above; here, $v_{\text{crit}} \equiv \sqrt{2GM_*/3R_p}$ is the critical rotation velocity at which the equatorial centrifugal force balances gravity. The underlying star has a mass $M_* = 1.35 M_\odot$, polar radius $R_p = 2.4 R_\odot$ and 'non-rotating' effective temperature $T_{\text{eff},0} = 10,000$ K, these parameters being chosen to coincide with those given by DM04 for the star M3-17. The model star is viewed equator-on, and we normalize all spectra to have a unit flux at 4,200 Å.

It is clear that the synthetic spectra are all similar longward of the Balmer discontinuity at 3,647 Å (see below) but that the magnitude of the jump – which we characterize throughout via the ratio $\Delta_B \equiv f_{4,200}/f_{3,630}$ between the continuum fluxes at 4,200 Å and 3,630 Å³ – varies noticeably with the rotation rate. In interpreting this behaviour, we recall that the spectrum of a rotating star is a composite, made up from contributions covering a range of effective temperatures and gravities. To illustrate the sensitivity of the Balmer jump against such variation in temperature and gravity, Fig. 2 plots Δ_B as a function of both T_{eff} and $\log g$, for a spectrum synthesized from a non-rotating plane-parallel atmosphere model.

The temperature dependence of Δ_B (left-hand panel) exhibits a sharp peak around $T_{\text{eff}} \sim 8,500$ K; at temperatures cooler than this turnover, the appearance of H^- bound-free opacity – which preferentially absorbs continuum photons toward longer wavelengths in the optical and UV (see, e.g. Fig. 8.3 of Gray 1992) – tends to suppress the flux redward of the Balmer discontinuity, resulting in a reduction of Δ_B . Likewise, at temperatures hotter than 8,500 K, the progressive depopulation of the $n = 2$ (Balmer ground-state) level of neutral hydrogen removes bound-free continuum opacity blueward of the discontinuity, again resulting in a reduction of Δ_B .

Similar behaviour is exhibited in the gravity dependence of the Balmer jump (right-hand panel of Fig. 2); H^- number densities are enhanced at high gravities, due to the corresponding increase in electron density, while

³ These points being chosen as well separated from spectral lines

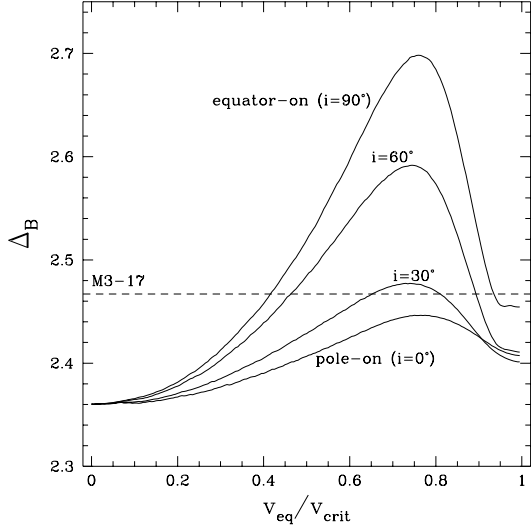


FIG. 3.— The Balmer jump magnitude Δ_B plotted as a function of rotation rate $v_{\text{eq}}/v_{\text{crit}}$, for the stellar model representative of M3-17 (see text). Data for different inclinations are shown; the horizontal dashed line indicates the jump magnitude observed in M3-17.

$n = 2$ level populations are depleted at low gravities, due to the reduction in collisional recombinations which replenish these populations. Together, these processes are responsible for the decline in Δ_B toward both low and high g .

In Fig. 3, we illustrate how the combined $T_{\text{eff}}/\log g$ sensitivities of the Balmer-jump magnitude come together in a rotating star, by plotting Δ_B as a function of rotation rate. We use the same stellar parameters as previously, but in the present case show data for both pole- and equator-on aspects. In each, Δ_B increases steadily up to a rate $v_{\text{eq}}/v_{\text{crit}} \sim 0.77$, due to the reduction in equatorial effective temperature and gravity from their non-rotating values $T_{\text{eff}} = 10,000$ K, $\log g_{\text{eff}} = 3.81$. At this point, the equatorial reduction of T_{eff} and g_{eff} is so pronounced that the low temperature/gravity regime of Δ_B is reached, and the magnitude of the Balmer jump then decreases rapidly toward even-higher v_{eq} . However, in every case, Δ_B for the rotating models is larger than in the non-rotating limit.

How then does rotation change the flux distribution redward of the Balmer Jump? In Fig. 4, we present a color-color diagram of the rotating models. The fluxes in the three photometric bands (centered at 3660Å, 4200Å and 5450Å) are averaged over 120Å, 80Å and 120Å widths respectively, and we use the zero-point magnitudes from Bessell Castelli & Plez (1998) – this is exactly the same as the procedure used DM04 to allow a direct comparison to be made. A grid of non-rotating model atmospheres is plotted (dotted lines) for temperatures between 8,500K–12,000K, and for $\log g = 2.5$ –5.0. Also we have calculated pole-on and equator-on rotating atmosphere models (for $v_{\text{eq}}/v_{\text{crit}} = 0.0$ –0.9 in steps of 0.1) for the [4200]–[5450] extreme blue edge of the non-rotating grid. The equator-on models (filled circles) sweep down and to the right (almost appearing like models becoming cooler at constant $\log g$), with the lower-temperature models eventually sweeping upward in a broad “u” shape. The loci of the pole-on models

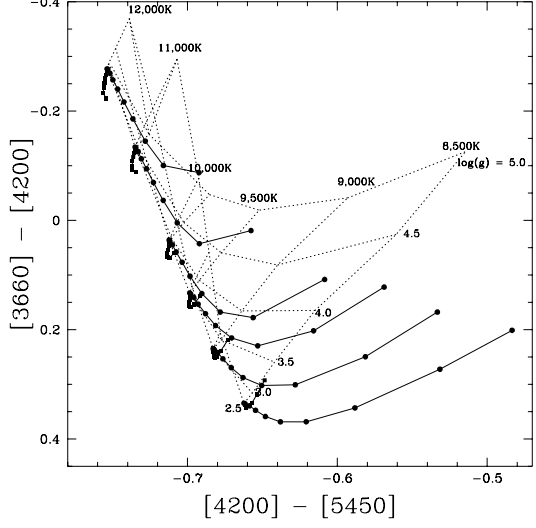


FIG. 4.— Color-color figure for both rotating and non-rotating atmosphere models. The dotted lines (with effective temperatures and gravities marked) correspond to models with zero rotation. The solid lines correspond to models with rotation rates of $v/v_{\text{crit}} = 0.0$ –0.9 in steps of 0.1 for pole-on (squares) and equator-on (circles) models.

(filled squares) initially move vertically down with increasing rotation (i.e. no change in the [4200]–[5450]) with the cooler models then reversing their track in a “v” shape. The maximum change in [3660]–[4200] becomes more pronounced for higher temperature models, reaching 0.06mag for the 12,000K model.

Two conclusions can be drawn from this figure: first, that for pole-on models, rotation can cause the Balmer jump (signified by the [3660]–[4200] color) to be too large whilst keeping the [4200]–[5450] color constant; second, if they are rotating, stars can exist with colors which are apparently inconsistent with non-rotating model atmospheres (i.e. the lower left-hand extremum of the non-rotating atmosphere grid is extended a little). Finally we note that the position of a star in the color-color plane does not yield a unique pair of effective temperature and gravity values – two color measurements cannot produce three unique values of effective temperature, gravity, and rotation.

4. APPLICATION TO M3-17

The observed projected rotation velocity of M3-17, $v \sin i = 200 \pm 50$ kms⁻¹, along with the stellar parameters furnished by DM04, implies that this object is a rapid rotator, having $v_{\text{eq}} \sin i / v_{\text{crit}} = 0.75 \pm 0.18$. The Balmer jump magnitude derived from the *HST* spectrum of this object is $\Delta_B = 2.47$, a value that we indicate in Fig. 3 by the horizontal dashed line. Clearly, there are multiple rotating models that can fit the observations, without the need to invoke a circumstellar disc; for example, a match to Δ_B can be achieved with an edge-on ($i = 90^\circ$) model rotating at $v_{\text{eq}}/v_{\text{crit}} \approx 0.4$ or 0.9, and other solutions can be found at lesser inclinations.

We further illustrate this point in Fig. 1, where we plot the archival spectrum of M3-17 over our model data. The non-rotating synthetic spectrum clearly has a surfeit of continuum flux shortward of the Balmer discontinuity, which led DM04 to diagnose the presence of a circumstellar disc. However, our equator-on rotating models

at $v_{\text{eq}}/v_{\text{crit}} = 0.4$ and 0.9 clearly provide a good fit to the continuum flux, suggesting that rotation alone may suffice to explain the Balmer jump. In support of this conclusion, we note that the rotational reddening of the Paschen continuum, as seen for the equator-on curves in Fig. 4, actually enables the rotating models to fit the observed [4200]-[5450] color of M3-17 *better* than the non-rotating model of the same temperature. We do observe that our models are unable to reproduce the strengths of the Balmer-series absorption lines seen redward of 3,647Å; this problem reflects the fact that we specify the model temperature *a priori* from that of DM04. The issue can be resolved by allowing $T_{\text{eff},0}$ (and other parameters) to vary under the control of a suitably-chosen fitting statistic. However, we do not undertake such fine tuning here, because we are not attempting to derive exact atmospheric parameters for M3-17 here. Rather, our objective is to highlight that high rotation has a significant effect on the continuum, and may mimic the presence of an obscuring disk.

5. DISCUSSION & SUMMARY

Using a spectral synthesis approach that correctly treats oblateness and gravity darkening, we have demonstrated that apparent flux deficits shortward of the Balmer discontinuity can be attributed wholly to rapid rotation. This casts doubt on the disc hypothesis advanced by De Marco et al. (2004) to explain the Balmer jump anomalies seen in the spectra of BSs. At least in the case of rapid rotator M3-17 ($v \sin i = 200 \pm 50 \text{ km s}^{-1}$), the continuum is well fit by our model, leaving little reason to invoke the presence of a disc.

⁴ By this, we mean models that do not include oblateness or gravity darkening.

In addition to M3-17, five other stars (out of a total of 50) in the DM04 sample show Balmer jumps that are enhanced with respect to non-rotating models⁴. Of these five, only NGC6751-11 has a measured (upper limit) projected rotation velocity, $v \sin i < 50 \text{ km s}^{-1}$. Due to the unknown projection factor $\sin i$, the upper limit on the intrinsic equatorial velocity v_{eq} may be much larger, and it is entirely possible that, along with the remaining objects with anomalous Balmer jumps, this star is a rapid rotator.

Accordingly, Balmer jump anomalies seen in BSs may *all* be attributable to rapid rotation. This hypothesis is lent some support by the fact that the proposed formation mechanisms for BSs – collisions or mass transfer – both involve the deposition of significant amounts of angular momentum on the star, thereby spinning it up (see, e.g., Pols & Marinus 1994).

On a final note, we stress that we do not (and cannot) rule out the possibility of discs around BSs. Indeed, observations of emission lines in these objects, bearing a close resemblance to those seen in Be stars (see Mermilliod 1982), indicate that there almost certainly *are* circumstellar discs around some of them. However, the present paper demonstrated why Balmer jump anomalies cannot be used as a clear and unambiguous diagnostic for BS discs.

RHDT acknowledges support from PPARC and from NSF grant AST-0097983. We thank the referee for their useful comments on the submitted paper.

REFERENCES

Bellazzini, M., Fusi Pecci, F., Messineo, M., Monaco, L., & Rood, R. T. 2002, AJ, 123, 1509
 Bessell, M.S., Castelli, F., & Plez B. 1998, A&A, 333, 231
 Cranmer, S. R. 1996, PhD thesis, University of Delaware
 Davies, M. B., Piotto, G., & de Angeli, F. 2004, MNRAS, 349, 129
 De Marco, O., Lanz, T., Ouellette, J. A., Zurek, D., & Shara, M. M. 2004, ApJ, 606, L151
 Deng, L., Chen, R., Liu, X. S., & Chen, J. S. 1999, ApJ, 524, 824
 Gray, D. F. 1992, *The Observation and Analysis of Stellar Photospheres*, 2nd edn. Cambridge: Cambridge University Press
 Kurucz, R. 1993, CD-ROM No. 16. Smithsonian Astrophysical Observatory, Washington D.C.
 Livio, M. 1993, in ASP Conf. Ser. 53, *Blue Stragglers*, ed. R. E. Stoffer, San Francisco: ASP, 3
 Mermilliod, J.-C. 1982, A&A, 109, 37
 Pols, O. R., & Marinus, M. 1994, A&A, 288, 475
 Shara, M. M., Saffer, R. A., & Livio, M. 1997, ApJ, 489, L59
 Sills, A., Faber, J. A., Lombardi, J. C., Rasio, F. A., & Warren, A. R. 2001, ApJ, 548, 323
 von Zeipel, H. 1924, MNRAS, 84, 665